Nanoscale

Accepted Manuscript

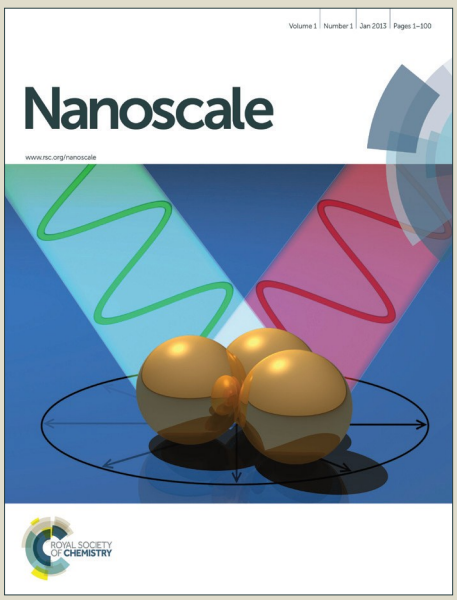

ROYAL SOCIETY OF CHEMISTRY

www.rsc.org/nanoscale

Journal Name

ARTICLE

Strongly Enhanced Ultraviolet Emissions of an Au@SiO_2/ZnO Plasmonic Hybrid Nanostructure

Received 00th January 20xx,
Accepted 00th January 20xx

DOI: 10.1039/x0xx00000x

www.rsc.org/

Li Wang,[a,b] Xiaodong Wang,[a,b] Shengcheng Mao,[a,b] Hua Wu,[c] Xia Guo,[c] Yuan Ji,[a,b*] and Xiaodong Han,[a,b*]

We present the surface plasmon polariton (SPP)-enhanced ultraviolet (UV) emissions of an Au@SiO_2/ZnO hybrid nanostructure. We achieved approximately 20- and 8-fold enhancements of the UV-emitting intensities from Au-SPP coupled nanometre- and micrometre-scaled ZnO wires through an optimized 5 nm-thick SiO_2 spacer compared to that obtained from bare ZnO on a Si substrate without SPP coupling. Cathodoluminescence measurements and simulations demonstrated that the plasmonic hybrid nanostructure enables the strong localization of the SPP field, resulting in significantly enhanced UV emissions. This plasmonic structure paves the way to nanoscale UV-optical lasers and sensors.

Introduction

ZnO is a strong ultraviolet (UV) luminescent material with a wide bandgap energy of 3.37 eV and a large exciton binding energy of 60 meV.[1,2] ZnO nanowires and microwires are one of the most promising integrated configurations for future nanolasers, biosensors, nano-optoelectronic devices, and photocatalysts.[3-6] The cathodoluminescence (CL) spectra of ZnO exhibit a near-band emission (NBE) in the UV range and visible emission in the green range. However, surface defect states in ZnO, such as oxygen vacancies, lower the light-emitting efficiency of photoelectric devices. Previously reported techniques for improving the UV-emissions of the ZnO structure include thermal annealing and the applications of ceramic, metal and polymeric surface coatings.[7-14]

In recent years, surface plasmon polariton (SPP)-coupled ZnO nanostructures have been observed to enhance UV-light emissions significantly.[15-23] SPPs are electromagnetic waves that propagate along a metal-dielectric interface at visible to infrared wavelengths.[24,25] The SPP field enhances the luminescence properties of nanostructures and nanocomponents because of strong coupling between photons and metal plasmons induced by optical localization. The coupling efficiency can typically be reduced by surface defects in ZnO nanostructures and ohmic losses in metals.[23,26] A semiconductor-insulator-metal (SIM) hybrid structure for SPP-coupling optical enhancement has been proposed, where a nanometre-scale low-refractive-index insulating spacer (e.g., MgF_2, SiO_2, PMMA, LiF, or Al_2O_3) is placed between the metal and semiconductor. Experiments and simulations have demonstrated that the SIM nanostructure enables energy storage in the non-metallic regions, resulting in enhanced SPP-field localization.[27-31] For instance, Volker J. Sorger et al. reported a UV-enhancement up to 5-fold from Ag@PMMA/ZnO.[30] Lawrie et al. demonstrated 1.45-fold and 1.8-fold UV-light enhancements from Au@MgO/ZnO and Ag@MgO/ZnO multilayer structures.[32] Yu-Hsun Chou et al. demonstrated a 20-fold UV enhancement from Ag@SiO_2/ZnO multilayer structures.[33] Several reports on SPP-coupling ZnO systems for UV-light enhancement are summarized in Table 1. The nature of enhanced UV emissions from the plasmonic-coupling MIS nanostructure with ZnO nanowires as UV nanolasers must be further explored.

In this work, we developed an Au-plasmon enhanced Au@SiO_2/ZnO hybrid structure that consists of ZnO nanowires/microwires separated from a Au film by a nanoscale dielectric SiO_2 spacer. We choose Au as the SPP metal due to its good coupling with ZnO NWs and chemical stability. Furthermore, Au is well known for its resistance to oxidation.[34] We achieved a ~20-fold enhancement in the UV-emission intensity from Au-SPP coupled ZnO NWs through an optimized 5 nm-thick SiO_2 spacer (Table 1). We explain the strong coupling geometry in the plasmonic hybrid configuration by varying the thickness of SiO_2 spacer and the size of ZnO NWs to enhance and modulate the UV emissions. We also investigated the effects of incident electrons on the UV enhancement of plasmonic nanostructure.

[a] Institute of Microstructure and Property of Advanced Materials, Beijing University of Technology, Beijing, 100124, P.R. China.
[b] Beijing Key Lab of Microstructure and Property of Advanced Material, Beijing University of Technology, Beijing, 100124, P.R. China.
[c] College of Electronic Information & Control Engineering, Beijing University of Technology, Beijing, 100124, P.R. China.
E-mail: jiyuan@bjut.edu.cn; xdhan@bjut.edu.cn; Fax: +86-10-67396087; Tel:+86-10-67396087

Table 1 Comparison of SPP-coupling ZnO systems with and without a dielectric spacer layer.

SPP-ZnO system	SPP-material	Dielectric spacer	UV-enhancement	References
Au@SiO_2/ZnO NW*	Au film	SiO_2 (*h******: 5 nm)	20-fold	Present work
Au/ZnO NR*	Au NPs**	w/o	4-fold	[10]
Au/ZnO NW*	Au NPs**	w/o	2-fold	[11]
Graphene/ZnO nano film	SG***	w/o	5-fold	[12]
Graphene/ZnO nano film	GO****	w/o	2.79-fold	[13]
Au/graphene/ZnO MW*	Au NP(s)**	w/o	4-fold	[14]
Ag/ZnO NR*	Ag NPs**	w/o	5-fold	[16]
Pt/ZnO NR*	Pt NPs**	w/o	12-fold	[18]
Au/ZnO NW*	Au NPs**	w/o	5-fold	[19]
Au/ZnO nano film	Au NPs**	w/o	15-fold	[23]
Ag@PMMA/ZnO NW*	Ag film	PMMA (*h*:10 nm)	5-fold	[30]
Au@MgO/ZnO Nano film	Au film	MgO (*h*: 20 nm)	1.45-fold	[32]
Ag@MgO/ZnO Nano film	Ag film		1.8-fold	
Ag@SiO_2/ZnO NW*	Ag film	SiO_2	20-fold	[33]

*NW: nanowire, NR: nanorod, MW: Microwire.
**NPs: nanoparticle.
***SG: single graphene.
****GO: grapheme oxide.
******h*: dielectric spacer thickness.

Experimental section

Sample preparation

The undoped ZnO nanowires/microwires (NWs/MWs) with a [0001]-orientation were fabricated by physical vapour deposition without a catalyst. The diameter of the wires was from ~300 nm to 3 μm. First, a 60 nm-thick Au film was deposited on a *p*-type Si (100) substrate by magnetron sputtering. An amorphous SiO_2 layer was then deposited on the Au film using the plasma enhanced chemical vapour deposition (PECVD). The thickness of the SiO_2 layer (*h*) was 5, 10, 20, or 100 nm. In the cathodoluminescence (CL) measurements for individual ZnO wires, the ZnO N&MWs were randomly dripped on the SiO_2 layer and on the Si (100) substrate without a SiO_2 layer and Au film for comparison.

Sample characterization

The measurement system was a spatially resolved CL spectroscope (Gatan Mono 3 Plus) combined with a field-emission environmental scanning electron microscope (FEI Quanta 600F ESEM). The ESEM-CL system provided a technical advantage for the observation and measurement of nanostructures with a high spatial resolution (1.2 nm) and a high spectral precision (0.66 nm). The experimental conditions of the ESEM and CL spectrometer included an accelerating voltage of 5-30 kV, a beam current of 10^{-8} -10^{-10} A, a working distance of 12.6 mm, and a photo multiplier tube detector (PMT) with a grating of 1,200 l/mm. The detection wavelength of the PMT detector ranged between 200 and 930 nm (UV to IR range).

To compare the influence of the thickness of the dielectric SiO_2 spacer on the UV emissions of ZnO wires, we selected ZnO wires with similar diameters from randomly dispersive wires on the SiO_2 layer. For CL measurements, the permissible errors of the diameter were ± 10 nm and ± 0.05 μm for NWs and MWs, respectively. We measured ZnO wires with diameters ranging from 300 nm to 1.6 μm and obtained CL results for 300 nm, 500 nm, and 1.6 μm wires. To reduce the influence of wire defects on the corresponding comparisons of the NBE intensity, we obtained a panchromatic CL

image, selected a homogeneously light-emitting area in an individual wire, and then collected a CL spectrum from this area.

Results and discussion

Fig. 1a shows the secondary electron (SE) images of ZnO wires randomly distributed on the SiO_2 layer of the Au@SiO_2/ZnO hybrid structure. The inset is a diagram of the plasmonic hybrid structure. Fig. 1b shows a ~500 nm ZnO wire, which lies on the SiO_2 layer. The SiO_2 layer is located beneath the ZnO and above the Au film and functions as a low-permittivity dielectric material to store SPP electromagnetic energy. We modulated the thickness of the SiO_2 spacer (h), the diameter of the ZnO wire (d), and the energy of the incident electrons (E_0) to enhance the UV-emitting intensity of the ZnO wires. For comparison, the ZnO wires on a Si substrate without any SPP coupling were also analysed.

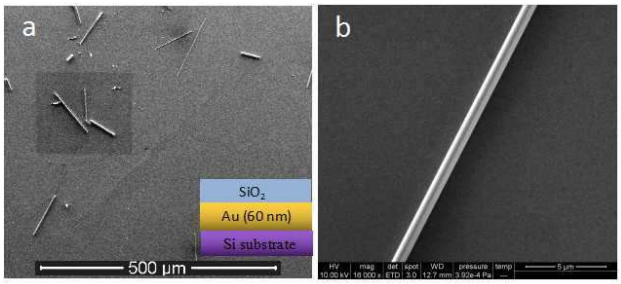

Fig. 1 SE images of the ZnO wires on the SiO_2 layer of the Au@SiO_2/ZnO hybrid structure. (a) ZnO wires randomly distributed on the SiO_2 layer. Inset is the diagram of the plasmonic hybrid structure. (b) A ~500 nm ZnO wire on the SiO_2 layer.

Fig. 2 illustrated a series of NBE peaks from a Au@SiO_2/ZnO hybrid nanostructure, where ~300 nm ZnO wires and a SiO_2 spacer with a thickness of h = 5, 10, 20, and 100 nm were used. The E_0 was 10 keV. When h was decreased from 100 to 5 nm, the NBE peaks were enhanced approximately 20-fold relative to those of bare ZnO NWs without any SPP coupling. Here, we define an enhancement factor (R_{NBE}) for the NBE emission as $R_{NBE} = I^{h}_{NBE} / I^{Si-sub}_{NBE}$, where I^{Si-sub}_{NBE} and I^{h}_{NBE} are the NBE intensity from the hybrid structure with ZnO wires and different dielectric layer thicknesses (h) and the NBE intensity of the bare ZnO wires on a Si substrate without plasmonic coupling, respectively. The R_{NBE} values were approximately 20-, 2.8- and 1.8-fold enhancements for h = 5, 10 and 20 nm compared to that of the ~300 nm ZnO on a Si substrate. The results suggest that the Au-SPP energy was effectively confined as the dielectric thickness was decreased. In contrast, the UV-enhancement of this plasmonic nanostructure was negligible when h > 20 nm. Moreover, the UV peaks located at 387 nm did not move when the thickness of the dielectric spacer was changed.

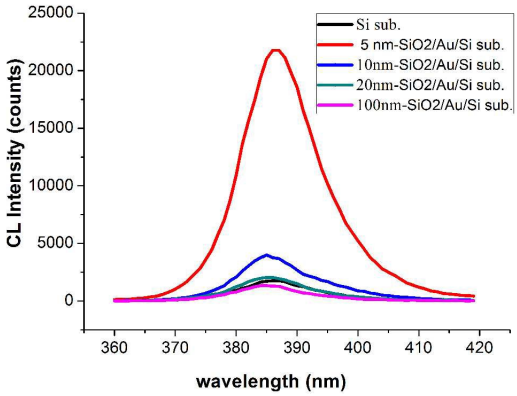

Fig. 2. UV peaks from the Au@SiO_2/ZnO hybrid structure with ~300 nm ZnO wires, where the thickness of the SiO_2 spacer (h) was 5, 10, 20, and 100 nm. The electron energy (E_0) was 10 keV.

A series of UV peaks from the plasmonic structure with ~1.6 μm ZnO wires are presented in Fig. 3 (h = 5, 10, 20, and 100 nm; E_0 = 10 keV). The trends of the UV enhancement were similar to those observed for the plasmonic structure with ~300 nm ZnO wires (Fig. 2). However, the R_{NBE} values significantly decreased, i.e., R_{NBE} = 8.4, 8.5, 4.7 and 3.5 for h = 5, 10, 20, and 100 nm, respectively. When h > 100 nm, the UV peaks weakened considerably, which suggested that SPP-coupling effect faded before reaching the ZnO/SiO_2 interface. Moreover, the UV peaks showed a red shift, i.e., from 387 nm for ~300 nm ZnO to 392 nm for ~1.6 μm ZnO. The bandgap narrowed for the shrunken nanowires because of the quantum confinement effect.

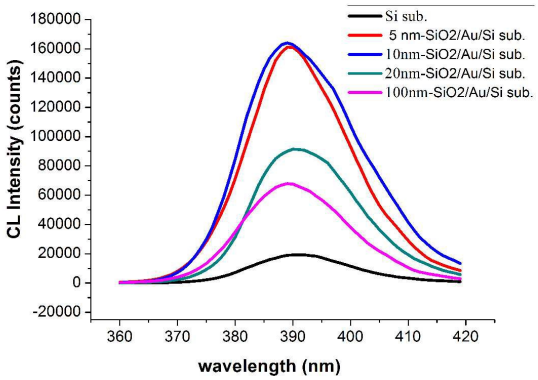

Fig. 3. UV peaks from the Au@SiO_2/ZnO hybrid structure with ~1.6 μm ZnO wires (h = 5, 10, 20, and 100 nm; E_0 = 10 keV).

Similarly, the SiO_2 spacer (h)-modulated UV-emitting intensity from the plasmonic structure with ~500 nm ZnO wires is shown in Fig. 4. Compared to the R_{NBE} values of ~300 nm and ~1.6 μm ZnO wires, the R_{NBE} values of the ~500 nm ZnO wires were intermediate, i.e., R_{NBE} = 10, 3.8, 1.8, and 1.02 for h = 5, 10, 20, and 100 nm, respectively.

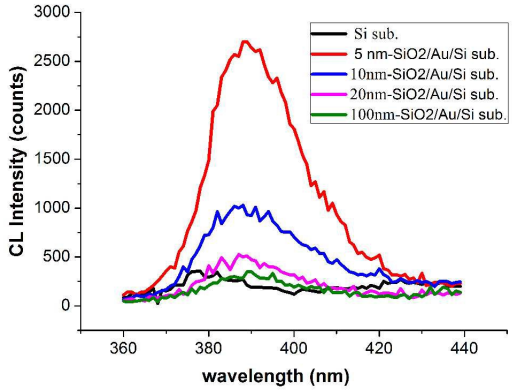

Fig. 4. UV peaks from the hybrid structure with ~500 nm ZnO wires (h = 5, 10, 20, and 100 nm; E_0 = 10 keV).

To determine the NBE-emitting nature of Au plasmons coupled with ZnO photons, we compared the enhancement factors (R_{NBE}) achieved with this plasmonic structures, as shown in Fig. 5. The R_{NBE} strongly increased when both the thickness of the dielectric layer (h) and the size of the ZnO wires (d) were decreased. Maximal UV enhancements of 20-fold (d ≈ 300 nm) were achieved for h = 5 nm, whereas the enhancements achieved were 10-fold for d ≈ 500 nm and 8.4-fold for d ≈ 1.6 μm. The results demonstrate that the shrunken geometric configuration of the hybrid structure led to a strong coupling in the metal-dielectric interface and to an UV-enhancement in the plasmonic nanostructure.

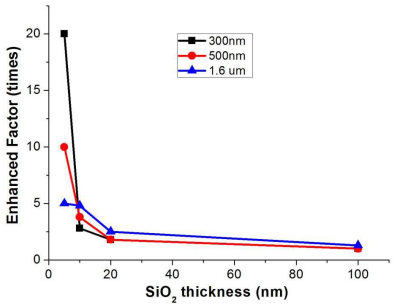

Fig. 5. Enhancement factors (R_{NBE}) achieved with Au@SiO_2/ZnO hybrid structures as a function of the thickness of the SiO_2 spacer and the diameter of the ZnO wires (h = 5, 10, 20 and 100 nm; E_0 = 10 keV).

Fig. 6 shows the panchromatic images of the ZnO wires. No visible defects were present in the ~300 nm ZnO wire (Fig. 6a). In contrast, more structural defects existed in the ~1.6 μm ZnO, as shown by an arrow (Fig. 6b). The crystal defects increased with increasing diameters of the wires, resulting in a decrease in the UV-emitting enhancement.

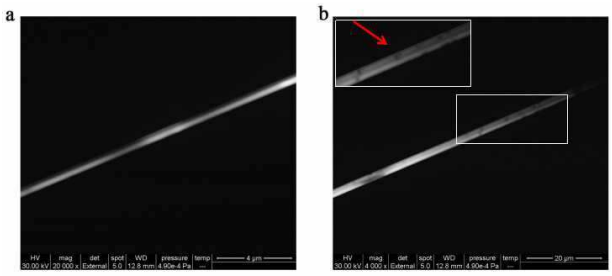

Fig. 6. Panchromatic CL images of ZnO wires in the plasmonic structures: (a) a ~300 nm ZnO wire and (b) a ~1.6 μm ZnO wire.

Next, we considered the penetration depth of surface plasmons fringing into the dielectric layer (Z), which can be expressed by Eq. (1).[14]

$$Z = \lambda / 2\pi \left[\left(\varepsilon'_{SiO_2} - \varepsilon'_{Au} \right) / \varepsilon'^{2}_{Au} \right]^{1/2} \quad (1)$$

where ε'_{SiO2} and ε'_{Au} are the real parts of the dielectric constants of SiO_2 and Au, respectively, and λ is the wavelength of ZnO (λ = 390 nm). The Z was calculated to be ~100 nm, which supports the results of our CL measurements, i.e., the SPP-coupled UV emissions fade as the thickness of the dielectric spacer increases to 100 nm.

Furthermore, we used the finite-difference time-domain (FDTD) simulations to evaluate the distribution of SPP field intensity (|E(x,y)|) in the Au@SiO_2/ZnO plasmonic nanostructure with various thicknesses of the SiO_2 spacer. Fig. 7 shows that the SPP-field intensity is dependent on both the thickness of the dielectric SiO_2 layers (h) and the diameter of the ZnO NWs (d). The FDTD simulations agree with the CL measurements. First, the strongest SPP-field intensity was obtained when the SiO_2 spacer was h = 5 nm. The SPP-field intensity in the SiO_2 spacer became stronger with decreases in the dielectric spacer h from 100 to 5 nm, whereas it became weaker with decreases in h from 5 to 2 nm (Fig. 7a-e). The enhanced SPP field with decreases in the dielectric spacer from 100 to 5 nm resulted in increases in the resonance energy localization by coupling between excitons of the ZnO and plasmons of the Au. As a result, the UV-emission was enhanced (Figs. 2-4). When the dielectric spacer reduced further from 5 to 2 nm, the SiO_2 layer formed an island-like discrete film. The decayed SPP-field was mainly attributed to the hot electron transfer from ZnO to Au, resulting in a decrease in the SPP-field intensity[31]. Second, the SPP-field intensity became stronger with decreases in d from ~500 to ~300 nm when h = 5 nm (Fig. 7b,f). This finding supports the notion that the SPP electric energy can be effectively confined in the thinner dielectric layer with shrunken nanowires. The results of the simulations indicate that the strong localization of the SPP electromagnetic energy originates from the nanometre-scaled dielectric and semiconductor structures and enables effective enhancements of the UV luminescence of ZnO nanowires.

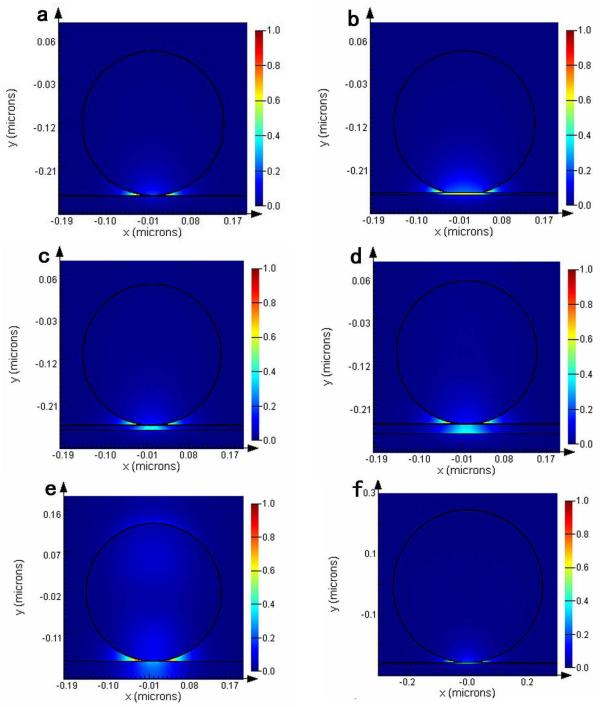

Fig. 7. FDTD simulations of the distribution of SPP field intensity (|E(x,y)|) in the Au plasmonic hybrid structure in the x-y plane. In the maps, black circles represent the profiles of the ZnO wires, and the two horizontal black lines represent the thickness of the SiO_2 layer. The wavelength was 390 nm, and the thickness of the Au film was 60 nm. (a-e) a ~300 nm ZnO wire with *h* = 2, 5, 10, 20 and 100 nm. (f) a ~500 nm ZnO wire with *h* = 5 nm.

Moreover, we consider a good fit of incident electron energy (E_0) for plasmonic-coupled NBE enhancement of the intensity. Here, we designated R_{NBE} as the E_0-dependent factor, i.e., $R_{NBE} = I_{NBE}^{E_0} / I_{NBE}^{E_0=3keV}$, where $I_{NBE}^{E_0}$ and $I_{NBE}^{E_0=3kV}$ are the NBE intensity of ZnO wires at a given E_0 value and at E_0 = 3 keV, respectively. Fig. 8 shows the UV enhancement (R_{NBE}) with the plasmonic structure (*h* = 5 nm) and the UV intensity (I_{NBE}) without any plasmonic structure for ZnO wires with E_0 ranging from 3 to 30 keV.

Fig. 8a shows the R_{NBE} of the ~300 nm ZnO wires and ~1.6 μm ZnO wires. Notably, the maximum R_{NBE} values of both the ~300 nm ZnO and ~1.6 μm ZnO wires were observed to occur at 10 keV, corresponding to the maximum UV-emitting enhancements. For the ~300 nm ZnO wires, the R_{NBE} values were approximately 20-fold higher at 10 keV, whereas they were approximately 7- and 6-fold enhancements at 5 and 15 keV, respectively, compared to that at 3 keV.

The phenomena should be further evaluated by the effect of the penetration depth of incident electrons on the CL spectra. The Monte Carle modulations indicated that the penetration depth of the beam energy into the Au@SiO_2/ZnO structure was approximately 0.9, 1.9, 2.8, and 4.9 μm for 5, 10, 15, and 20 keV, respectively. The modulations conditions included a ~1.6 μm ZnO wire, beam energies of 5, 10, 15 and 20 keV, an incident electron number of 32,000, and thicknesses of 100 and 60 nm for the SiO_2 layer and Au film. The results suggested that the penetration depth was equivalent to the total thickness of the ZnO/SiO_2/Au multilayer structure at 10 keV, whereas it was less than or higher than this total thickness at 5 or 15 keV. Then, the corresponding R_{NBE} values displayed a notable difference.

Five-fold enhancements of RNBE could be obtained at 5 keV as Monte Carlo modulations typically underestimate the beam energy corresponding to the maximum CL intensity.35 For this reason, the minority carrier diffusion and secondary luminescence in matter are not accounted for in the simulations. As the CL could be generated at the location of the e-h pair recombination, the CL probe could be broadened and reach the bottom of the multilayer structure at 5 keV. In contrast, a notable decrease in RNBE with increasing beam energy from 10 to 30 keV could be attributed to the reduction in the proportion of the multilayer structure to the interaction volume of the incident electrons. The most suitable beam energy for the maximum NBE- enhancement in the plasmonic structure was E0 = 10 keV.

Fig. 8b-c shows the maximum INBE of 300 nm wires and 1.6 m ZnO wires, respectively, on the Si substrate without a plasmonic structure. The maximum INBE values of the 300 nm ZnO wire and 1.6 m ZnO wire were located at 10 and 15 keV, respectively. The maximum RNBE value occurred at 10 keV for the 300 nm ZnO wire, whereas the maximum INBE value occurred at 15 keV for the 1.6 m ZnO wire (Figs. 8a and 8c). These results are related to the NBE emission mechanisms from the different geometric configurations of the ZnO wire. The NBE enhancement of the intensity (RNBE) is mainly attributed to the plasmonic geometric configuration for SPP-excited coupling resonance between Au plasmons and ZnO photons, related to the SiO2 spacer and Au/SiO2 interface. In contrast, the NBE intensity (INBE) is mainly attributed to an electron-excited spontaneous recombination-luminescence process, related to the interaction volume of incident electrons with matter.

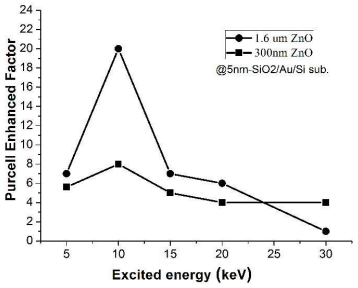

(a)

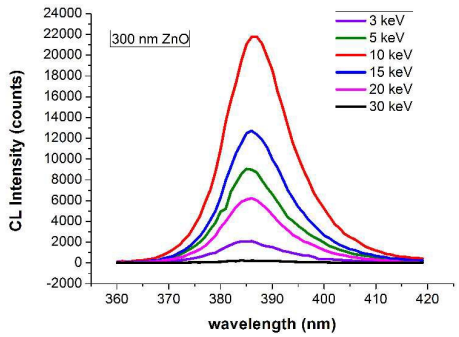

(b)

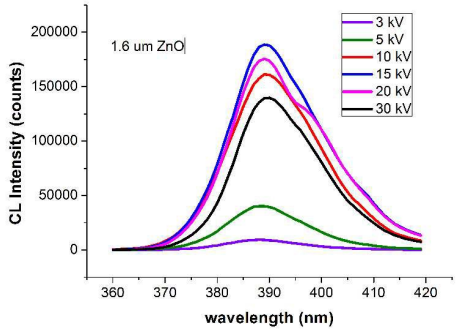

(c)

Fig. 8. NBE enhancement factor (R_{NBE}) and NBE intensity (I_{NBE}) vs. incident electron energy (E_0): (a) R_{NBE} vs. E_0 of ~300 nm ZnO wires and ~1.6 μm ZnO wires from the plasmonic structure; (b) and (c) I_{NBE} vs. E_0 of ~300 nm and ~1.6 μm ZnO wires from the Si substrate (E_0 = 3, 5, 10, 15, 20 and 30 keV, h = 5 nm).

Conclusions

In summary, we achieved approximately 20-fold and 8-fold enhancements in the UV-emitting intensity from ~300 nm ZnO wires and ~1.6 μm ZnO wires, respectively, in the Au@SiO_2/ZnO hybrid structure with a 5 nm-thick SiO_2 spacer compared to that obtained from the bare ZnO wires on a Si substrate without SPP-coupling. The suitable geometric configuration of the plasmonic nanostructure includes a SiO_2 spacer thickness of 5–20 nm and a ZnO nanowire diameter of several hundred nanometres. An incident electron energy of 10 keV is the most suitable for enhancing UV emissions in the plasmonic structure. The clear UV-emitting enhancement is attributed to the strong localization of coupling resonance between the Au plasmons and ZnO excitons. FDTD simulations support the CL measurements, which demonstrate that the plasmonic hybrid structures enable enhancements in SPP-field localization and energy storage. The UV-enhanced plasmonic nanostructure could be used to develop nanoscale UV-optical lasers and sensors.

Acknowledgements

This work was supported by the National Natural Science Foundation (11004004, 11327901, 11127404), the Beijing Municipal Natural Science Foundation (1112004), the Project of Construction of Innovative Teams and Teacher Career Development for Universities and Colleges Under Beijing Municipality (IDHT20140504), and the Importation and Development of High-Caliber Talents Project of Beijing Municipal Institutions (CIT&TCD201504013). The authors are grateful to Dr Z.G. Yan for the helpful discussions.

Notes and references

1 E. F. Schubert and J. K. Kim, *Science,* 2005, **308**, 1274-1278.
2 D. Panda and T. Y. Tseng, *J. Mater. Sci.,* 2013, **48**, 6849–6877.
3 H. Q. Yan, J. Johnson, M. Law, R. R. He, K. Knutsen, J. R. Mckinney, J. Pham, R. Saykally and P. D. Yang, *Adv. Mater.* 2003, **15**, 1907–1911.
4 M. Law, D. J. Sirbuly, J. C. Johnson, J. G. Goldberger, R. J. Saykally and P. D. Yang. *Science*. 2004, **305**, 1269–1273.
5 R. Konenkamp, R. C. Word and M. Godinez, *Nano Lett*, 2005, **5**, 2005–2008.
6 Z. Q. Cheng, M. Y. Yu, G. X. Yang, and L. J. Kang, *Cryst. Eng. Comm.* 2015, **17**, 1765-1768 .
7 X. Q. Meng, H. W. Peng, Y. Q. Gai and J. B. Li, *J. Phys. Chem. C.*, 2010, **114**, 1467–1471.
8 M. T. Hill, Y. S. Oei, B. Smallbrugge, Y. C. Zhu, T. De Vries, P. J. V. Veldhoven, F. W. M. Van Otten, T. J. Eijkemans, J. P. Turkiewicz, H. de Waardt, E. J. Geluk, S. H. Kwon, Y. H. Lee, R. N. Mtzel and M. K. Smit, *Nature Photon,* 2007, **1**, 589–594.
9 W. L. Barnes, *J. Optics. Opt. A: Pure Appl. Opt*. 2006,8, S87–S93.
10 Y. Lin, C. X. Xu, J. T. Li, G. Y. Zhu, X. Y. Xu, J. Dai and B. P. Wang. *Adv.Optical Mater.,* 2013, **1**, 940–945.
11 T. Chen, G. Z. Xing, Z. Zhang, H. Y. Chen and T. Wu, *Nanotechnology,* 2008, **19**, 435711 .
12 S. W. Hwang, D. H. Shin, C. O. Kim, S. H. Hong, M. C. Kim, J. Kim, K. Y. Lim, S. Kim, S. H. Choi, K. J. Ahn, G. Kim, S. H. Sim and B. H. Hong. *Phys. Rev. Lett.,* 2010, **105**, 127403.
13 K. Kim, S. M. Lee, Y. S. Do, S. Ahn and K. C. Choi. *J. Appl. Phys.* 2013, **114**, 074903.
14 R. Liu, X. W. Fu, J. Meng, Y. Q. Bie, D. P. Yu and Z. M. Liao. *Nanoscale,* 2013, **5**, 5294–5298.
15 F. Han, S. M. Yang, W. X. Jing, K. C. Jiang, Z. D. Jiang and H. Liu. *Optical express,* 2010, **22**, 11436-11445.
16 P. Sunghoon, A. Soyeon, Y. H. Mun, H. W. Kim and C. M. Lee. *J Mater Sci: Mater. Electron*., 2013, **24**, 4906–4912.

17 M. Gwon, E. Lee, D. W. Kim and K. J. Yee. *Optical Express,* 2011, **19**, 5895-5901.

18 J. M. Lin, H. Yu, C. L. Cheng and Y. F. Chen, *Nanoparticles*, 2006, **17**, 4391- 4394.

19 K. Liu, Sakurai, Makoto., M. Y. Liao and M. J. Aono, *Phys. Chem.C.* 2010, **114**, 19835–19839.

20 K. Okamoto, I. Niki, A. Shvartser, Y. Narukawa and T. Mukai, *A. Scherer*. 2004, **3**, 601-605.

21 E. N. Economou, *Phys. Rev.* 1969, **182**, 539-554.

22 S. A. Maier and H. A. Atwater, *J. Appl. Phys*. 2005, **98**, 011101-1-10.

23 C. W. Lai, J. An and H. C. Ong, *APL,* 2005, **86**, 251105.

24 Dmitry Yu. Fedyanin, Alexey V. Krasavin, Aleksey V. Arsenin, and Anatoly V. Zayats, *Nano Lett*. 2012, **12**, 2459–2463.

25 Hongxing Xu, Mikael Kall, *Sensors and Actuators B*, 2002, **87,** 244–249.